Available online at www.sciencedirect.com
SCIENCE DIRECT®
Chemical Engineering and Processing 43 (2004) 305–316
Chemical Engineering and Processing
www.elsevier.com/locate/cep

Influence of unequal component efficiencies on trajectories during distillation of a homogeneous azeotropic mixture

J.A. Ojeda Nava, R. Krishna*

Department of Chemical Engineering, University of Amsterdam, Nieuwe Achtergracht 166, 1018 WV Amsterdam, The Netherlands

Received 8 November 2002; received in revised form 18 January 2003; accepted 20 February 2003

Abstract

The overall objective of this work is to examine the influence of interphase mass transfer on the composition trajectories in homogeneous azeotropic distillation. A total of 38 experiments were carried out in a bubble cap distillation column operated at total reflux with the system: water–ethanol–*tert*-butanol. The experiments were carried out in the two regions on either side of the distillation boundary connecting the ethanol–water and *t*-butanol–water azeotropes.

In order to model the composition trajectories, a rigorous nonequilibrium (NEQ) stage model is developed. The NEQ model incorporates the Maxwell–Stefan diffusion equations to describe the intraphase transfers in the vapor and liquid phases. The only adjustable parameter in the NEQ model is the size of the vapor bubbles on trays. A choice of a bubble diameter of 4 mm in the developed NEQ model gave the best agreement with the experimental results for all of the 38 experimental runs. The Murphree efficiencies of the constituents in the ternary mixture were found to be significantly different from one another for all the runs. In order to ascertain the influence of unequal component efficiencies on the column composition trajectories, the experimental results were also simulated with an equilibrium (EQ) stage model assuming a uniform, constant efficiency for all components on all the trays. The value of this constant efficiency for any experimental run was obtained by averaging the individual component efficiencies for all the three components on all the trays, calculated by the rigorous NEQ model. The predictions of the EQ model leads to significantly worse predictions of the column composition trajectories for each of the runs, when compared to the NEQ model. It is found that the column composition trajectories are significantly altered due to *differences* in the component efficiencies.

From a design view point, it is shown that for the water–ethanol–*tert*-butanol system, the attainment of a desired ethanol purity in the top product may require significantly larger number of stages than that anticipated by the EQ model incorporating constant component efficiencies.

Keywords: Azeotropic distillation; Residue curve maps; Maxwell–Stefan equations; Distillation boundary; Nonequilibrium stage; Equilibrium stage

1. Introduction

The traditional method for simulating distillation tray columns is based on the equilibrium (EQ) stage model wherein the vapor leaving any stage is assumed to be in equilibrium with the liquid leaving that stage through the downcomer. In practice, the contact time between the vapor and liquid phases is not long enough for equilibrium to be established and Murphree [1] was the first to provide a measure of approach to equilibrium by defining the *stage efficiency*:

$$E_i = \frac{y_{i,\mathrm{L}} - y_{i,\mathrm{E}}}{y_i^* - y_{i,\mathrm{E}}}, \quad i = 1, 2, \ldots, n \tag{1}$$

where the subscript i refers to species i in the n-component mixture, and the subscripts E and L refer to the entering and leaving streams on the stage (see Fig. 1). The y_i^* represent the compositions of the vapor that would be in equilibrium with the liquid leaving the tray. The mole fractions add to unity:

$$\sum_{i=1}^{n} y_{i,\mathrm{L}} = 1, \qquad \sum_{i=1}^{n} y_{i,\mathrm{E}} = 1, \qquad \sum_{i=1}^{n} y_i^* = 1 \tag{2}$$

and, consequently, only $n - 1$ of the Murphree stage efficiencies E_i are independent. For a binary mixture, $n = 2$, there is only one Murphree stage efficiency, that is equal

* Corresponding author. Tel.: +31-20-525-7007; fax: +31-20-525-5604.
E-mail address: krishna@science.uva.nl (R. Krishna).

0255-2701/$ – see front matter © 2003 Elsevier B.V. All rights reserved.
doi:10.1016/S0255-2701(03)00130-2

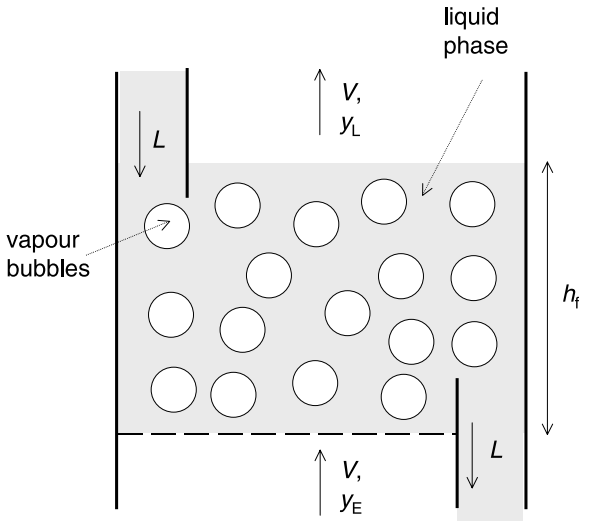

Fig. 1. Shematic of the bubble froth regime on the tray with two liquid phases.

for components 1 and 2:

$$E_1 = \frac{y_{1,L} - y_{1,E}}{y_1^* - y_{1,E}} = \frac{y_{2,L} - y_{2,E}}{y_2^* - y_{2,E}} = E_2 \tag{3}$$

When the number of components n is three or more; there is no requirement that the Murphree efficiencies E_i be equal to one another:

$$E_1 \neq E_2 \neq E_3 \cdots \neq E_n \tag{4}$$

There is a large body of experimental evidence for ternary distillation in the published literature to verify that component efficiencies are not equal to one another and that any of these efficiencies could vary from $-\infty$ to $+\infty$; see the comprehensive literature survey given in Chapter 13 of Taylor and Krishna [2]. Careful examination of the classic paper by Murphree [1] reveals that he appreciated Eq. (4) already in 1925: "For three-component mixtures the approach to equilibrium would not in general be equal for the two volatile components, ...". It is only several decades later that procedures for calculation of the component Murphree efficiencies were developed by adopting the Maxwell–Stefan (M–S) formulation [2–4] to describe intraphase mass transport. In the M–S diffusion formulation, chemical potential gradients are used as the driving forces for diffusion and a linear relation is postulated between the driving forces and the fluxes in the form

$$-\frac{x_i}{RT}\nabla\mu_i = \sum_{\substack{j=1\\ j\neq i}}^{n} \frac{x_j N_i - x_i N_j}{c_t Đ_{ij}} \quad i = 1, 2, \ldots, n, \tag{5}$$

where x_i represent the mole fraction in the fluid phase under consideration; N_i the molar fluxes; $Đ_{ij}$ the M–S diffusivities; $\nabla\mu_i$ the chemical potential gradients. It is of historical interest to note that Lewis and Chang [5], in 1928, were already aware of the usefulness of the Maxwell–Stefan formulation for modelling mass transfer on distillation trays.

Following the approach of Taylor and Krishna [2], we can also write the M–S formulation in terms of the phase mass transfer coefficients κ_{ij}:

$$\sum_{j=1}^{n} \Gamma_{ij}\,\Delta x_j = \sum_{\substack{j=1\\ j\neq i}}^{n} \frac{x_j N_i - x_i N_j}{c_t \kappa_{ij}}, \quad i = 1, 2, \ldots, n-1 \tag{6}$$

where Δx_i represents the differences in composition between the bulk fluid phase and the interface. The Γ_{ij} represent thermodynamic correction factors

$$\Gamma_{ij} = \delta_{ij} + x_i \frac{\partial \ln \gamma_i}{\partial x_j}, \quad i, j = 1, 2, \ldots, n-1 \tag{7}$$

Eq. (6) can be re-cast into $n-1$ dimensional matrix notation

$$N = c_t[k][\Gamma](\Delta x) \tag{8}$$

where $[k]$ is the $(n-1)\times(n-1)$ dimensional square matrix of mass transfer coefficients. For a ternary system, the four elements of $[k]$ can be determined explicitly from the following set of equations (for derivations see Taylor and Krishna [2]):

$$\begin{aligned} k_{11} &= \frac{\kappa_{13}[y_1\kappa_{23} + (1-y_1)\kappa_{12}]}{S} \\ k_{12} &= \frac{y_1\kappa_{23}(\kappa_{13} - \kappa_{12})}{S} \\ k_{21} &= \frac{y_2\kappa_{13}(\kappa_{23} - \kappa_{12})}{S} \\ k_{22} &= \frac{\kappa_{23}[y_2\kappa_{13} + (1-y_2)\kappa_{12}]}{S} \end{aligned} \tag{9}$$

where

$$S = y_1\kappa_{23} + y_2\kappa_{13} + y_3\kappa_{12} \tag{10}$$

Eqs. (8)–(10) show that flux of any species depends on the driving forces Δx_i of all the species present in the mixture. The extent of coupling depends inter alia on the *differences* in the transfer coefficients κ_{ij} of the binary pairs *i–j* in the mixture in either fluid phase. For a mixture made up of components that are similar in molecular size, shape, polarity and hydrogen bonding characteristics, coupling effects are expected to be minimal and the component efficiencies are nearly equal to one another. This is the case, for example, for distillation of close boiling hydrocarbon mixtures. On the other hand, for highly non-ideal mixtures of components with widely differing molar masses, coupling effects can expected to be very significant. The influence of diffusional coupling manifests itself in significant differences in the component E_i. For simulation of multicomponent distillation columns the M–S formulation has been incorporated into commercially available software packages such as RATEFRAC (marketed by Aspen Technology) and ChemSep (available through the CACHE corporation; see also http://www.chemsep.org). Such simulation models are usually called rate-based or nonequilibrium (NEQ) models. In industrial design it is much more common to adopt the

Table 1
NRTL parameters for binary mixtures at 101.3 kPa, taken from El Yafi et al. [7]

Component i	Component j	B_{ij} (K)	B_{ji} (K)	α_{ij}
Water	Ethanol	620.17	−20.46	0.3194
Water	*tert*-butanol	1122.14	209.54	0.4917
Ethanol	*tert*-butanol	250.99	−335.37	−0.1382

These parameters are used along with $G_{ij} = \exp(-\alpha_{ij}\tau_{ij})$ and $\tau_{ij} = B_{ij}/T$.

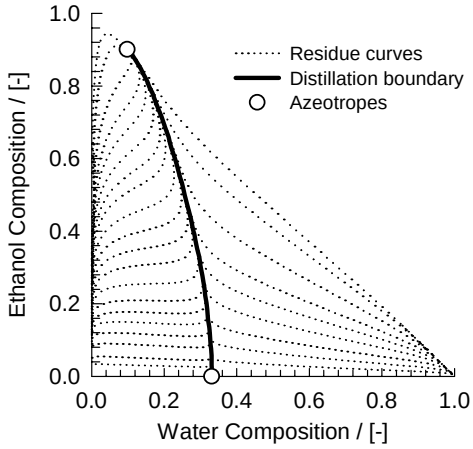

Fig. 2. Residue curve map for the water (1)–ethanol (2)–*tert*-butanol (3) system.

equilibrium (EQ) stage model with uniform and constant stage efficiencies for all components on all the trays.

Our major objective is to investigate the influence of interphase mass transfer on the composition trajectories in homogeneous azeotropic distillation in order to check whether unequal component efficiencies E_i can lead to significantly *different* results from those anticipated by an EQ stage model, with equal component efficiencies for *all* components. Towards this end, we performed experiments with the system: water (1)–ethanol (2)–*tert*-butanol (3) in a bubble cap tray distillation column. The choice of this ternary system was motivated by our earlier experiments with this system in a sieve tray column wherein we found that the component efficiencies were significantly different from one another [6]. The residue curve maps for this system, calculated with NRTL parameters [7], listed in Table 1, are shown respectively in Fig. 2. The residue curve map divides into two regions, separated by a distillation boundary, that connects the ethanol–water azeotrope with the *tert*-butanol–water.

2. Experimental set-up

The experiments were carried out in a laboratory-scale distillation column supplied by Schott Nederland B.V. (see Fig. 3). The double layered glass column with vacuum between the inner and outer shell contains a total condenser (stage 1), a partial reboiler (stage 12) and ten bubble cap trays (stages 2–11) for which the dimensions are detailed in Table 2 and pictured in Fig. 3. The distillation column is

Table 2
Bubble cap tray design of the laboratory-scale distillation column

Column diameter (mm)	50	Hole pitch (mm)	14.2
Tray spacing (mm)	46.2	Cap diameter (mm)	28.1
Number of flow passes	1	Skirt clearance (mm)	3
Liquid flow path length (mm)	30.8	Slot height (mm)	5
Downcomer clearance (mm)	3.9	Active area (of total area)	97.3%
Deck thickness (mm)	3	Total hole area (of total area)	8.27%
Hole diameter (mm)	14.2	Downcomer area (of total area)	1.35%
Weir type	Circular	Slot area (mm^2)	221
Weir length (mm)	18.2	Riser area (mm^2)	158
Weir height (mm)	9.2	Annular area (mm^2)	462
Weir diameter (mm)	5.8		

divided into two sets of five bubble cap trays by an intersection at which a continuous feed can be introduced to the column. Product streams can be tapped automatically from the condenser and manually from the reboiler. The glass distillation column has several small openings of 10 mm in diameter, which are sealed with Teflon-coated septa. These opening enable liquid and vapor samples to be withdrawn by means of a syringe. The column has a total height of 2160 mm and a 50 mm inner diameter.

The reboiler is placed in a heating mantle, which is connected with a PC provided with the required software (Honeywell: Windows NT Workstation 4.0; FIX MMI V 6.15/75-I/O-points run time; OPTO CONTROL rel.2.2a). By means of the PC, the reboiler temperature can be controlled as well as the feed- and product-flows. Furthermore, it provides an automatic safety shut down in case the column reboiler accidentally tends to dry up. The condenser is connected with a water tap which supplies cooling water to the glass cooling tubes inside the condenser.

A total of 38 experimental runs, indicated by R01–R38, under total reflux conditions and atmospheric pressure were carried out with the system water–ethanol–*tert*-butanol. The compositions of the vapor phase leaving the reboiler in all the 38 runs are indicated in Fig. 4a and b. Runs R01–R20 had their compositions located on the left of the distillation boundary and runs R21–R38 had their compositions on the right of the distillation boundary. For any given experiment, eight vapor and four liquid samples were taken from several stages (the sampling points are shown in Fig. 3) and the temperature profile was measured with PT 100 sensors. Each sample volume was intentionally kept small (100 μl) to prevent changes in the composition-profile during the entire experiment. The samples were first dissolved into a reference solvent, consisting of 1 vol.% *n*-propanol in 99 vol.% acetone, before injection into the Gas Chromatograph (type: GC8000-Top with pressure/flow control) by means of an autosampler (type AS800). The channel inside the GC is made of stainless steel and has a total length of 1 m and 0.3175 mm diameter. The carrier gas used was helium because of its high thermal conductivity and chemical inertness. By

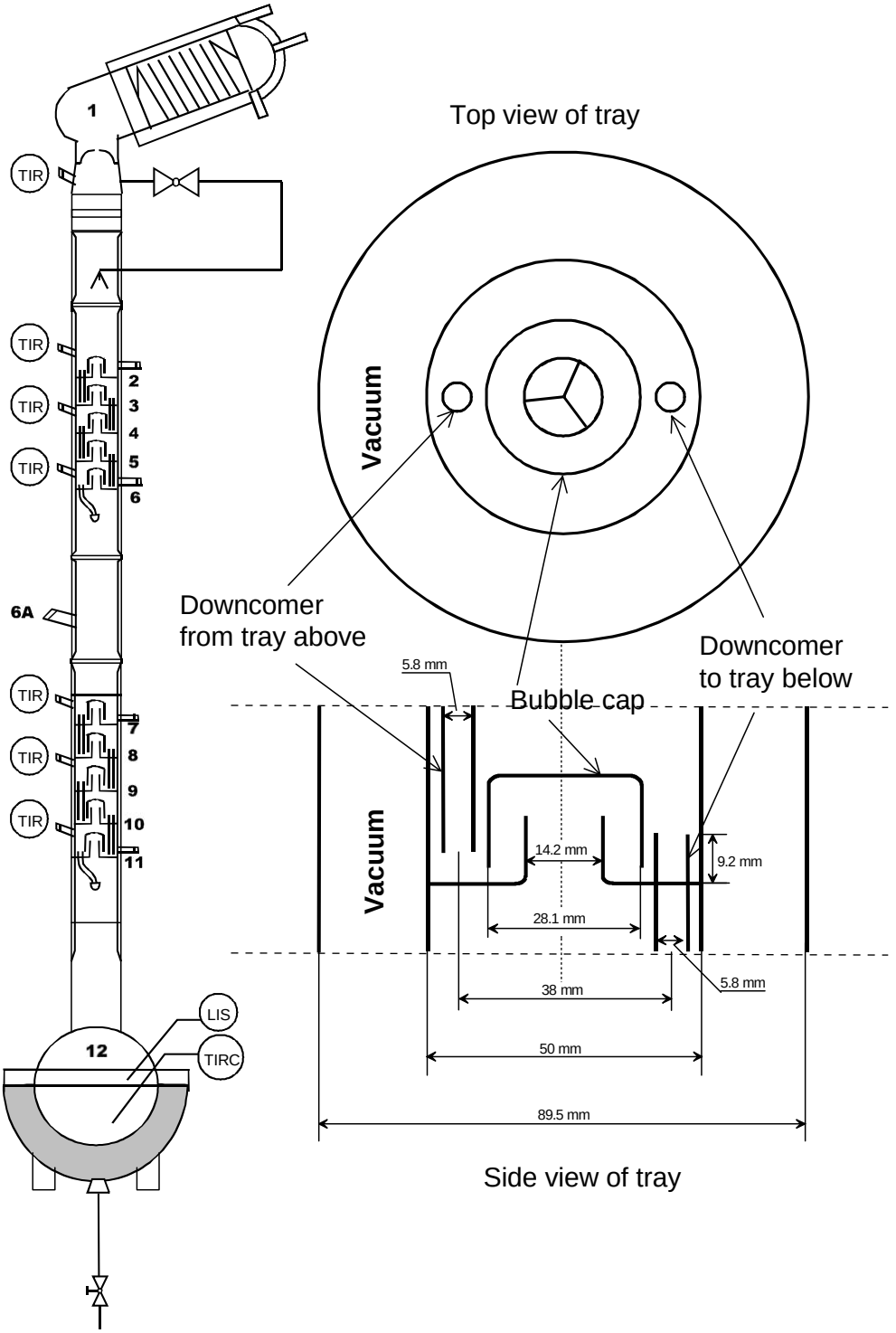

Fig. 3. Schematic of laboratory-scale distillation column. Includes total condenser (1), partial reboiler (12), 10 bubble cap trays (2–11) and 13 draw-off faucets, nine for vapor samples (V) and four for liquid samples (L). Details of bubble cap shown in the inset.

analyzing samples of pre-prepared, known, compositions, the GC was carefully calibrated. More detailed descriptions of the experimental set-up, measurement technique, GC analysis and composition determination, including pictures of the column and bubble cap trays are available on our web-site: http://ct-cr4.chem.uva.nl/distillation/.

3. NEQ model development

Before discussing the experimental results we summarize the details of the NEQ model. All our experiments were carried out in the bubbly froth regime. We assume the bubbles to be made up of uniform in size and having a diameter d_b.

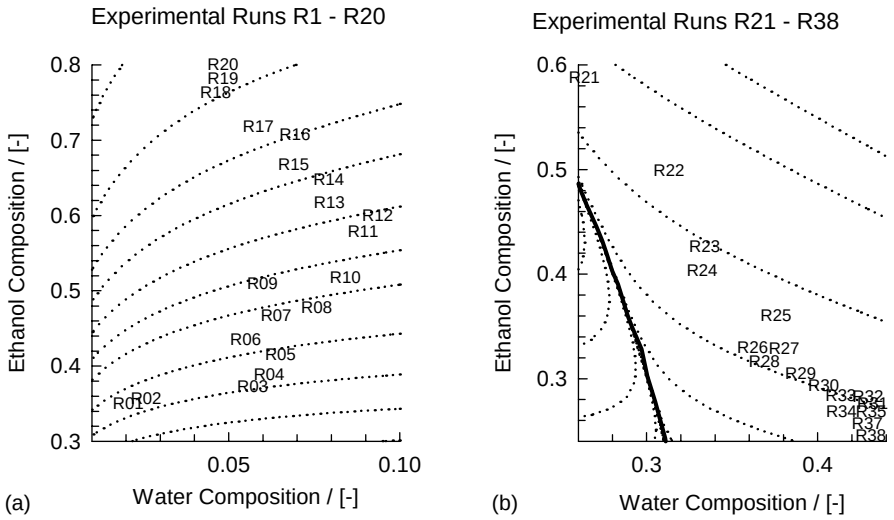

Fig. 4. Compositions of vapor leaving the reboiler in each of the 38 experimental runs. (a) Runs R01–R20 were performed on the left of the distillation boundary (b) runs 21–38 were performed on the right side of the distillation boundary.

We therefore have to reckon with two intraphase transfer processes: (1) transfer within the bubble, and (2) transfer within the continuous liquid phase; these transfer processes are pictured in Fig. 5.

In order to quantify the transfer processes, pictured in Fig. 5, we apply the treatment in earlier publications by Taylor et al. [2–4,8–16]. There are two transport resistances to reckon with. The transfer coefficients inside the rigid bubbles can be estimated from taking the corresponding Sherwood numbers to equal $2\pi^2/3$ following the development of Springer et al. [9–12]. The estimation of the transfer coefficients in the continuous liquid phase surrounding the bubble

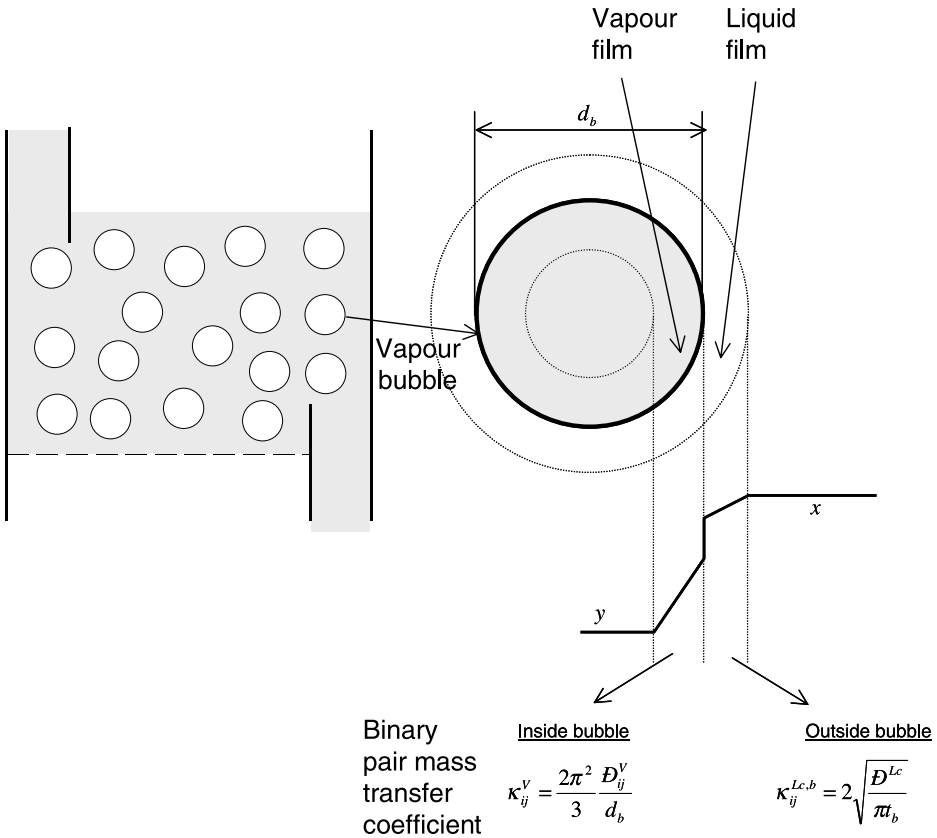

Fig. 5. Schematic showing the transfer resistances for distillation in the bubbly froth regime.

Table 3
Physical and transport properties per stage of run 09 for the water (1)–ethanol (2)–*t*-butanol (3) system obtained by NEQ model simulations (bubble diameter = 4.0 mm)

Stage no.	$\mathcal{Đ}^{V}_{1-2}$ (10^{-6} m^2 s^{-1})	$\mathcal{Đ}^{V}_{1-3}$ (10^{-6} m^2 s^{-1})	$\mathcal{Đ}^{V}_{2-3}$ (10^{-6} m^2 s^{-1})	$\mathcal{Đ}^{L}_{1-2}$ (10^{-9} m^2 s^{-1})	$\mathcal{Đ}^{L}_{1-3}$ (10^{-9} m^2 s^{-1})	$\mathcal{Đ}^{L}_{2-3}$ (10^{-9} m^2 s^{-1})	σ (10^{-2} N m^{-1})	ρ^{L} (kg m^{-3})	V_b (m s^{-1})	τ^{V} (s)
2	21.5	15.9	7.89	5.37	4.13	2.73	3.67	758	0.21	0.0440
3	21.5	15.9	7.9	5.38	4.18	2.74	3.62	756	0.21	0.0441
4	21.5	15.9	7.9	5.39	4.24	2.76	3.55	755	0.21	0.0443
5	21.5	15.9	7.9	5.43	4.32	2.78	3.47	753	0.21	0.0446
6	21.6	15.9	7.91	5.47	4.42	2.8	3.36	752	0.20	0.0449
7	21.6	15.9	7.91	5.53	4.54	2.83	3.24	750	0.20	0.0453
8	21.6	15.9	7.92	5.6	4.68	2.86	3.11	748	0.20	0.0458
9	21.6	16	7.93	5.67	4.83	2.89	2.98	745	0.20	0.0462
10	21.6	16	7.94	5.74	4.99	2.93	2.84	743	0.20	0.0467
11	21.7	16	7.95	5.8	5.15	2.97	2.72	741	0.19	0.0472

follows the penetration model:

$$\kappa^{L}_{ij} = 2\sqrt{\frac{\mathcal{Đ}^{L}_{ij}}{\pi t_b}} \tag{11}$$

where the contact time of the continuous liquid phase with gas bubbles, t_b is given by

$$t_b = \frac{d_b}{V_b} \tag{12}$$

The bubble rise velocity V_b is estimated using the Mendelson equation [17], recommended by Krishna et al. [18]:

$$V_b = \sqrt{\frac{2\sigma}{\rho^{L} d_b} + \frac{g d_b}{2}} \tag{13}$$

The calculation method of the transfer coefficients κ_{ij} for two transfer resistances is summarized in Fig. 5. The transfer coefficients are different for each of the three binary pairs 1–2, 1–2, and 2–3 in the ternary mixture. The binary pair κ_{ij} is obtained by substituting the appropriate binary pair M–S diffusivity $\mathcal{Đ}_{ij}$, in the fluid phase under consideration, into the relations presented in Fig. 5. For a typical run R09, to be discussed in detail below, the various parameter values on stages 2–11 have been listed in Table 3. The two transfer coefficient matrices $[k^{V}]$ and $[k^{L}]$ can then be calculated from Eqs. (9) and (10) by using the appropriate values of the bulk fluid phase compositions x_i and binary pair κ_{ij}.

The flux entering the vapor bubble can be expressed in terms of an overall matrix of mass transfer coefficients

$$N = c^{V}_{t}[K^{OV}](y^* - y) \tag{14}$$

where y^* is the composition of the vapor in equilibrium with the aqueous within the dispersed droplets. From the continuity relations for interphase mass transfer, the following expression can be derived for the overall transfer coefficient matrix $[K^{OV}]$:

$$[K^{OV}]^{-1} = [k^{V}]^{-1} + \frac{c^{V}_{t}}{c^{L}_{t}}[K_{eq}][k^{L}]^{-1} \tag{15}$$

The $[K_{eq}]$ represents the diagonal K-value matrix with elements

$$K_{eq} = \left(\frac{y_i}{x_i}\right)_{eq}, \quad i = 1, 2 \tag{16}$$

The next step in the model development is to integrate the flux expression for interphase transfer along the height of dispersion on the tray. We assume that the bubbles rise through the liquid in a plug flow manner and that liquid phase is well-mixed. The steady state component molar balance for vapor flow through the froth on the tray for three-component distillation is given by the two-dimensional matrix relation

$$V_b \frac{d(y)}{dh} = [K^{OV}](y^* - y)\frac{6}{d_b} \tag{17}$$

where d_b is the diameter of the bubbles rising in the froth with a rise velocity V_b. Eq. (17) can be re-written in terms of the overall number of transfer units for the vapor phase, $[NTU^{OV}]$:

$$\frac{d(y)}{d\xi} = [NTU^{OV}](y^* - y) \tag{18}$$

where $\xi = (h/h_f)$ is the dimensional distance along the froth and $[NTU_{OV}]$ is defined as

$$[NTU^{OV}] = [K^{OV}]\frac{6}{d_b}\tau_V \tag{19}$$

where the vapor residence time is determined from

$$\tau^{V} = \frac{h_f}{V_b} \tag{20}$$

where h_f is the height of dispersion (froth). The height of the dispersion on the tray is taken to be the height of the downcomer tube above the tray floor, i.e. 9.2 mm as seen in Fig. 3. This is a good approximation; any uncertainties in the value of h_f will be reflected in the choice of the bubble size.

Assuming that the $[NTU^{OV}]$ on a single stage is constant, Eq. (18) can be integrated using the boundary conditions

$$\begin{aligned} &\xi = 0 \text{ (inlet to tray)}, && y = y_E \\ &\xi = 1 \text{ (outlet of tray)}, && y = y_L \end{aligned} \tag{21}$$

to obtain the compositions leaving the distillation stage; detailed derivations are available in Taylor and Krishna [2]:

$$(y^* - y_L) = \exp[-[\mathrm{NTU}^{OV}]](y^* - y_E) \quad (22)$$

Introducing the matrix $[Q] \equiv \exp[-[\mathrm{NTUOV}]]$, we may re-write Eq. (22) in the form

$$(y_L - y_E) = [[I] - [Q]](y^* - y_E) \quad (23)$$

where [I] is the identity matrix. The limiting case of the EQ stage model is obtained when the NTU_{ij}^{OV} attain large values; [Q] reduces in this case to the null matrix and the compositions leaving the tray (y_L) are equal to (y^*), in equilibrium with the liquid leaving the tray. Substituting Eq. (15) in Eq. (19) gives us the $[\mathrm{NTU}^{OV}]$, required for calculation of the [Q] matrix in Eq. (23). We follow the procedure of Kooijman and Taylor [19] for implementation of the Eq. (23) in the stage-to-stage calculation.

The material balance relations outlined above need to be solved along with the enthalpy balance relations. The required heat transfer coefficients in the vapor phase are calculated from the heat transfer analogue of the mass transfer equations.

The entire set of material and energy balance equations, along with the interphase mass and energy transfer rate relations are then incorporated into a rigorous stage-to-stage model as described in Chapter 14 of Taylor and Krishna [2]; this chapter contains more exhaustive details of this model including sample calculations for binary and ternary mixtures.

The only adjustable parameter in the NEQ model developed above is the bubble diameter; this is obtained by fitting with the experimentally determined composition trajectories as explained below.

4. Experiments versus simulations

The operating pressure for all experiments was 101.3 kPa and the ideal gas law was used. Activity coefficients were calculated using the NRTL interaction parameters, specified in Table 1, and the vapor pressures were calculated using the Antoine equations. The vapor phase was assumed to be thermodynamically ideal. The column consists of 12 stages, including the total condenser (stage 1) and partial reboiler (stage 12). The reflux flow rate (0.003 mol/s) and the bottom flow rate (0.0 mol/s) were used for specifying the column-operations. Since the mass and heat transfer coefficients are independent on the internal flows, the composition and temperature profiles are not dependent on the precise value of the specified reflux flow rate.

Since the column is operated at total reflux, the reflux flow rate determined the inner flow rates of vapor and liquid phases on each stage. Simulation of total reflux operations is "complicated" by the fact that there is no feed to the column at steady-state. To overcome this problem we specify one of the experimentally determined compositions of the streams leaving or entering a stage as input parameter. The simulated composition profile of the total reflux run is forced to pass through this specified composition. The entire set of equations system was solved numerically by using the Newton's method [14]. The NEQ implementation is available in the software program ChemSep, developed by Taylor et al. [2,13–15]. Detailed information on ChemSep are available in the recent book by Kooijman and Taylor [20].

We illustrate our procedure by considering a specific run R09. The experimentally determined compositions of the vapor leaving the reboiler (stage 12) are, respectively for water, ethanol and *t*-butanol: 0.059831, 0.50905 and 0.431119. Using this composition as "input" to the NEQ model, simulations can be carried out to determine the composition trajectory along the height of the column for a variety of chosen bubble diameters. The simulation results for $d_b = 2$, 3, 3.5, 4, and 5 mm are shown in Fig. 6a. By minimizing the sum of the relative deviations between the experimentally determined vapor compositions and the simulated values:

$$\text{Percentage average deviation} = \sum_{i=1,2,3} \sum_{\text{stages}} \frac{y_{i,\text{expt}} - y_{i,\text{simulation}}}{y_{i,\text{expt}}} \left(\frac{1}{3}\right)\left(\frac{1}{7}\right) \times 100 \quad (24)$$

where the average deviation is determined for all three components and the seven experimentally measured vapor samples. We find that a bubble diameter of 4 mm gives the best fit, i.e. the minimum deviation; see Fig. 7. An alternative method for simulating the experiments is to use the vapor composition entering the (total condenser), V2, as "input" to the NEQ model. The experimentally determined compositions of the vapor entering the condenser, i.e. leaving stage 2 (V2) are, respectively for water, ethanol and *t*-butanol: 0.19977, 0.59749, and 0.20274. The simulation results for $d_b = 2$, 3, 3.5, 4, and 5 mm using the composition V2 as input are shown in Fig. 6b. The best fit bubble diameter is again found to be 4 mm; see Fig. 7.

A similar analysis was carried for each of the 38 experimental runs and it was found that in all cases the choice of 4 mm bubble size yields the best fit. Fig. 8 shows the comparison of experimentally determined composition trajectories, with those obtained from NEQ model, taking 4 mm bubble size and composition of the vapor leaving reboiler as input, for nine representative runs of the total of 38 runs. Run 22 is typical of the trajectories found on the right of the distillation boundary (see Fig. 4b) for runs R21–R38. We see from Fig. 8 that there is good agreement between the NEQ model and the experiments.

We now proceed to examine whether an EQ stage model, with uniform, constant, efficiency for all components is of adequate accuracy in describing the column trajectories. The first problem is to determine the uniform constant efficiency to use in the EQ stage simulations. For this purpose we consider the calculations of the Murphree component efficiencies using Eq. (1) where we use the NEQ model (with 4 mm bubble size) to determine the compositions entering

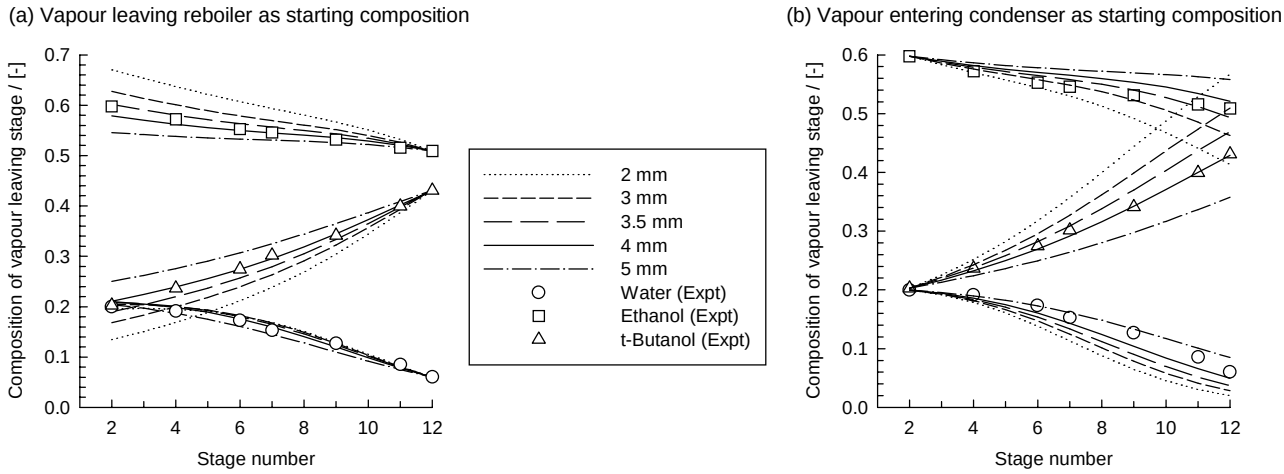

Fig. 6. Composition trajectories for run 09, calculated using (a) V12 and (b) V2 as starting compositions. NEQ model simulations for a variety of bubble sizes.

and leaving a particular stage. The calculations of E_i for three typical runs, R09, R01 and R22 are shown in Fig. 9. Consider run R09, ethanol is found to have the lowest efficiency, water the highest efficiency, and *t*-butanol has the intermediate efficiency. The differences in the values of the component Murphree efficiencies can be traced to the differences in the constituent vapor phase binary pair diffusivities, see Table 3. The vapor phase transport resistance is dominant and the differences in the vapor phase $Đ_{ij}$ induce significant off-diagonal elements in the $[k^V]$ matrix, following Eq. (9).

If we average the three component efficiencies for *all* the stages, we obtain the value of 0.624. This is the constant efficiency value we use in the EQ stage model in order to obtain a fair comparison with the NEQ model simulations. For run R01, the differences in the component efficiencies are even more pronounced than for run R09. For the run R22, the component efficiencies are closer together. The average stage efficiencies, for use in the EQ stage model are summarized in Fig. 10a. Simulations of the all the experiments with the EQ stage model using these efficiency values were carried out and the percentage average deviation, calculated using Eq. (24), are shown in Fig. 10b for the NEQ and EQ models. We note that for nearly all experiments the NEQ model yields a lower deviation from experiments. For the run R01 the EQ model shows a much higher percentage average deviation than the NEQ model; the reason for this can be traced to the fact that the component efficiencies for this run are significantly different from one another; see Fig. 9b. The composition trajectories calculated with the EQ stage model are indicated by the dashed lines in Fig. 8 for the nine selected runs R01, R07, R09, R11, R12, R13, R14, R18, and R22. We see that EQ model does not even qualitatively follow the corrected experimental trends for all runs expecting R22. For run 22 the differences in the component Murphree efficiencies are small (see Fig. 9c) and this is reflected in a small difference in the trajectories of the NEQ and EQ models.

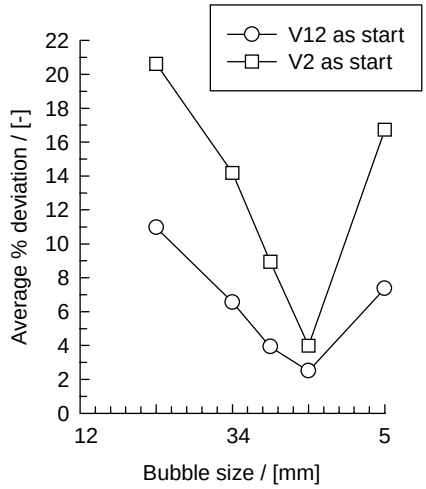

Fig. 7. NEQ model simulations for run 09 for a variety of bubble sizes, using V12 and V2 as starting compositions. The *y*-axis represents the percentage average deviation of the simulated vapor compositions from the experimentally determined values.

5. Consequences of unequal component efficiencies in column design

In column design, the objective is to determine the number of stages required for a specified separation task. For illustration, let us consider the conditions corresponding to run R09, where the vapor compositions leaving the reboiler are, respectively for water, ethanol and *t*-butanol: 0.059831, 0.50905, and 0.431119. Let us demand that the composition of ethanol at the top of the column should be at least 0.8. What is the number of stages required for this column, operated at total reflux? Simulations with the NEQ model (4 mm bubble size) and the EQ model (with constant efficiency = 0.625) are shown in Fig. 11. We see that the EQ model requires 26 stages to reach an ethanol composition of 0.8 at

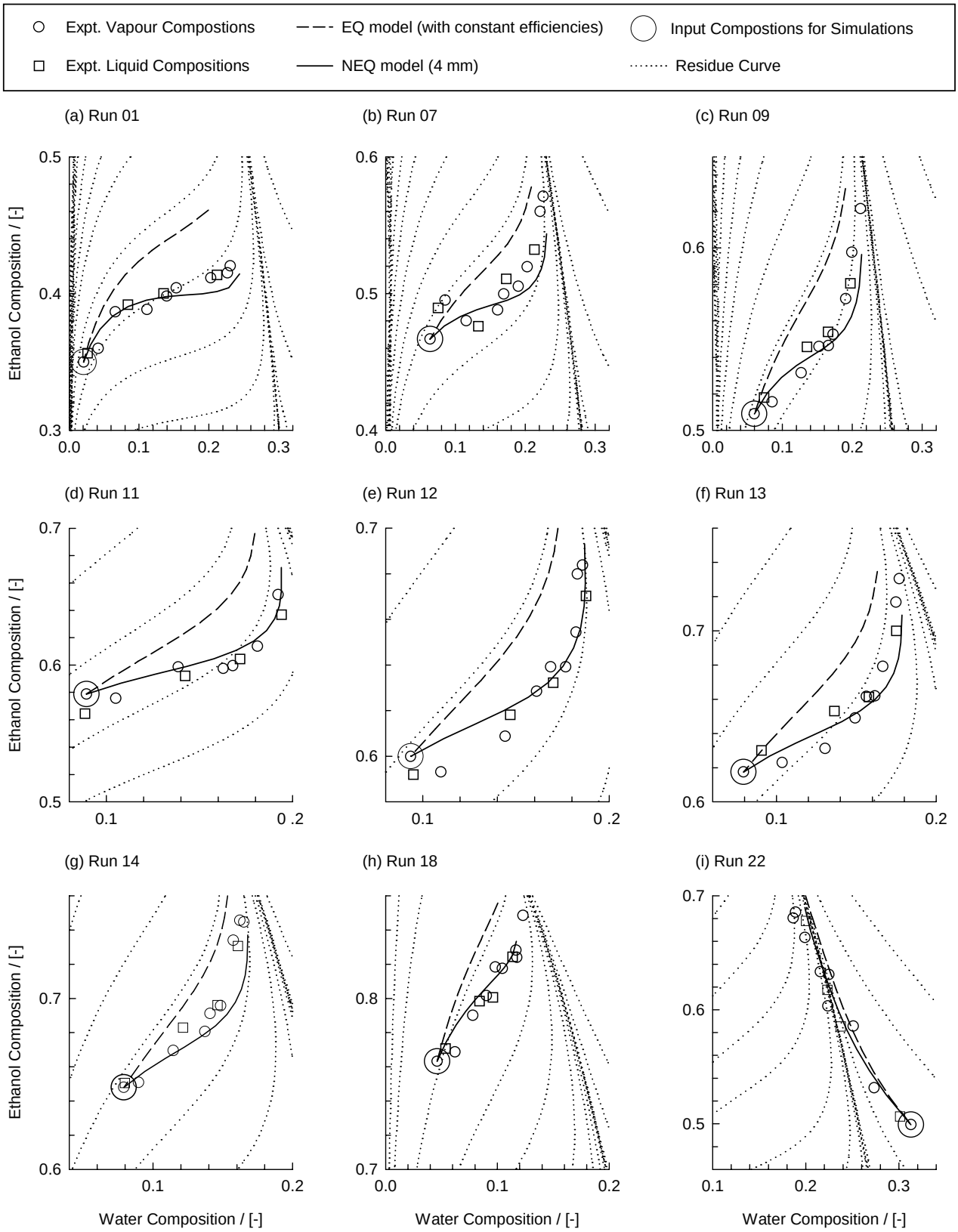

Fig. 8. Experimental results (open circles for vapor samples and open squares for liquid samples) showing the column composition trajectories. Also shown are the simulation results showing the trajectories calculated by the NEQ stage model (4 mm bubble size) and the EQ stage model (with uniform constant efficiencies for all components on all stages). The large open circles represent the experimental composition (vapor leaving reboiler, V12) specified as "input" in the simulations.

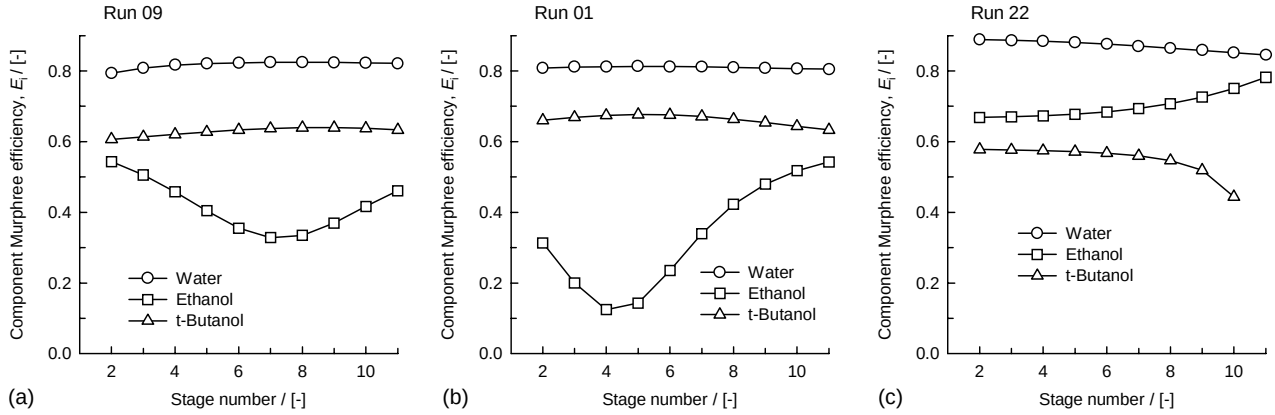

Fig. 9. Component Murphree efficiencies for R09, R01, and R22 on various stages, calculated from NEQ model (4 mm bubble size).

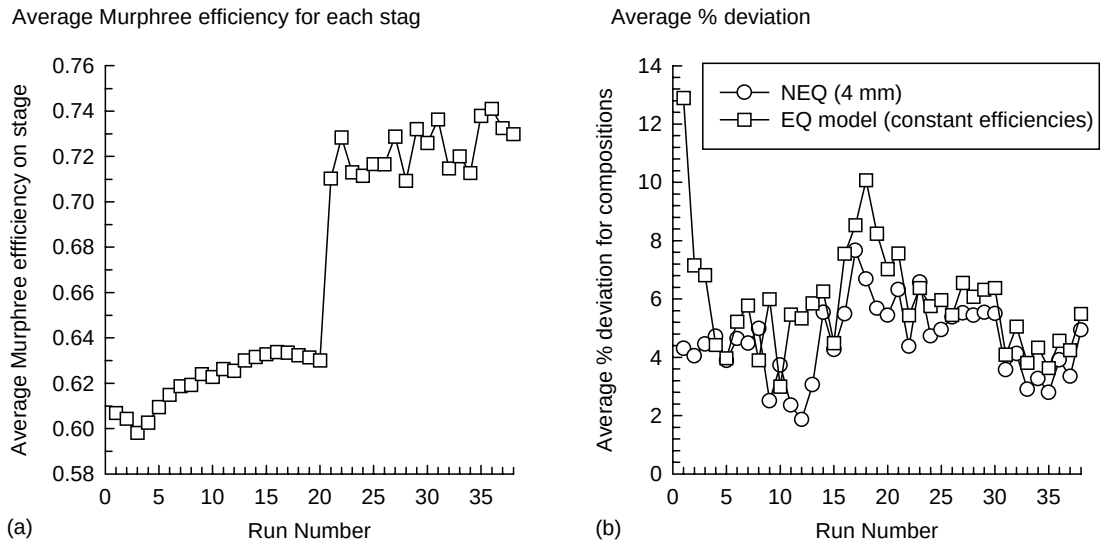

Fig. 10. (a) Average Murphree efficiencies for each experimental run; (b) percentage average deviation for NEQ model and EQ model for each experimental run.

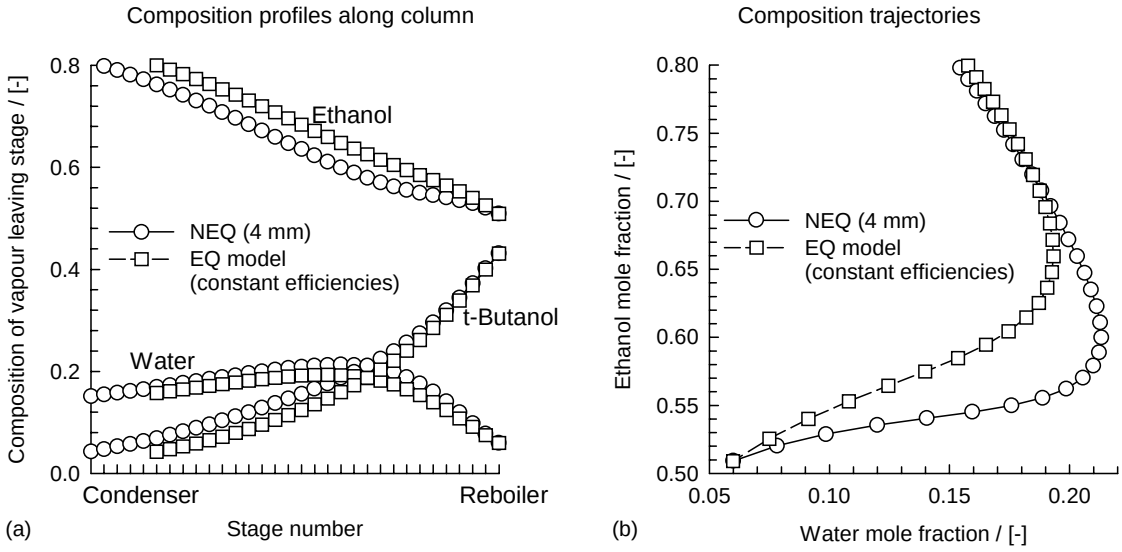

Fig. 11. (a) Stage composition profiles for NEQ and EQ stage models along column height; (b) composition trajectories for NEQ and EQ stage models.

the top, whereas the NEQ model requires 31 stages for this task. Use of the EQ model could lead to severe underdesign, that is to be ascribed to differences in the component efficiencies. The reason for this underdesign is to be found in the fact that the component efficiencies, as predicted by the NEQ model are different for each component; the component efficiency for ethanol is the lowest of the three (see Fig. 9a). The EQ model, assuming all component efficiencies to be equal to one another, overestimates the separation power of the column with respect to enrichment of ethanol; this leads to underestimation of the number of stages required to achieve a desired purity of ethanol at the top of the column.

6. Conclusions

The following major conclusions can be drawn from the work presented in this paper.

1. For the water–ethanol–*t*-butanol system, the NEQ model is superior to the EQ model in its ability to predict the column composition trajectories. The percentage average deviations (defined by Eq. (24)) is significantly lower for the NEQ for the 38 experimental runs (see Fig. 10b).
2. The differences between the composition trajectories predicted by the NEQ and EQ models is to be ascribed to the differences in the component efficiencies of water, ethanol, and *t*-butanol; see Fig. 9. The differences in the component E_i can be traced to significant differences in the vapor phase binary diffusivities $Đ_{ij}^{V}$ (see Table 3).
3. From a design point of view, use of the EQ stage model can lead to significant underestimation of the required number of stages to achieve a desired level of purity of ethanol in the top product (see Fig. 11).

The overall conclusion to be drawn from this work is that for reliable simulation of homogeneous azeotropic distillation systems, we must adopt a rigorous NEQ stage model.

Acknowledgements

The authors acknowledge a grant from the Netherlands Organization for Scientific Research (NWO), Chemical Sciences Division (CW), for investigations on three-phase distillation. The authors are Dr. R. Baur for assistance with the distillation code used in this work.

Appendix A. Nomenclature

B_{ij}	NRTL parameters; see Table 1 (K)
c_i	molar concentration of species i (mol m^{-3})
c_t	mixture molar density (mol m^{-3})
d_b	bubble diameter (m)
$Đ_{ij}$	Maxwell–Stefan diffusivity for pair i–j (m^2 s^{-1})
E_i	component Murphree stage efficiency (dimensionless)
G_{ij}	NRTL parameters; see Table 1 (dimensionless)
g	acceleration due to gravity (m s^{-2})
h	distance along froth height (m)
h_f	height of dispersion (m)
k_{ij}	element for matrix of multicomponent mass transfer coefficient (m s^{-1})
$[k]$	matrix of multicomponent mass transfer coefficients (m s^{-1})
$[K_{eq}]$	diagonal matrix of K-values (dimensionless)
$[K^{OV}]$	matrix of multicomponent overall mass transfer coefficients (m s^{-1})
$[NTU^{OV}]$	matrix of overall number of vapor phase transfer units (dimensionless)
n	number of species in the mixture (dimensionless)
S	parameter defined in Eq. (10) (m s^{-1})
Sh	sherwood number (dimensionless)
t_b	liquid–bubble contact time (s)
T	temperature (K)
V_b	single bubble rise velocity (m s^{-1})
x_i	liquid composition for component i (dimensionless)
y_i	vapor composition for component i (dimensionless)

Greek letters

α_{ij}	non-randomness parameter in NRTL equation, see Table 1 (dimensionless)
κ_{ij}	binary Maxwell–Stefan mass transfer coefficients (m s^{-1})
μ^L	liquid viscosity (Pa s)
μ_i	molar chemical potential (J mol^{-1})
ρ^L	density of the liquid (kg m^{-3})
σ	surface tension (N m^{-1})
τ^V	vapor phase residence time (s)
τ_{ij}	NRTL parameters; see Table 1 (dimensionless)
ξ	dimensionless distance along dispersion or column height, dimensionless

Subscripts

b	referring to a bubble
f	referring to the froth
i	component index
j	stage index
L	referring to the continuous liquid phase
OV	overall parameter referred to the vapor phase
ref	reference
V	referring to the y-phase (vapor)

Superscripts

$*$	referring to equilibrium state
L	referring to the continuous liquid phase
V	referring to the vapor phase

References

[1] E.V. Murphree, Rectifying column calculations with particular reference to *n*-component mixtures, Ind. Eng. Chem. 17 (1925) 747–750.

[2] R. Taylor, R. Krishna, Multicomponent Mass Transfer, Wiley, New York, 1993.

[3] R. Krishna, J.A. Wesselingh, The Maxwell–Stefan approach to mass transfer, Chem. Eng. Sci. 52 (1997) 861–911.

[4] J.A. Wesselingh, R. Krishna, Mass transfer in multicomponent mixtures, Delft University Press, Delft, 2000.

[5] W.K. Lewis, K.C. Chang, Distillation III: the mechanism of rectification, Trans. Am. Inst. Chem. Eng. 21 (1928) 127–138.

[6] R. Krishna, H.F. Martinez, R. Sreedhar, G.L. Standart, Murphree point efficiencies in multicomponent systems, Trans. Inst. Chem. Eng. 55 (1977) 178–183.

[7] A.H. El Yafi, H. Martinez, D.M.T. Newsham, N. Vahdat, Vapor–liquid equilibria for ethanol + *t*-butanol + water and methanol + isopropanol + water at atmospheric pressure, J. Chem. Thermodyn. 8 (1976) 1061–1073.

[8] R. Baur, R. Taylor, R. Krishna, J.A. Copati, Influence of mass transfer in distillation of mixtures with a distillation boundary, Chem. Eng. Res. Des. 77 (1999) 561–565.

[9] P.A.M. Springer, R. Krishna, Crossing of boundaries in ternary azeotropic distillation: influence of interphase mass transfer, Int. Commun. Heat Mass Transf. 28 (2001) 347–356.

[10] P.A.M. Springer, B. Buttinger, R. Baur, R. Krishna, Crossing of the distillation boundary in homogeneous azeotropic distillation: influence of interphase mass transfer, Ind. Eng. Chem. Res. 41 (2002) 1621–1631.

[11] P.A.M. Springer, S. van der Molen, R. Krishna, The need for using rigorous rate-based models for simulations of ternary azeotropic distillation, Comput. Chem. Eng. 26 (2002) 1265–1279.

[12] P.A.M. Springer, S. van der Molen, R. Baur, R. Krishna, Experimental verification of the necessity to use the Maxwell–Stefan formulation in describing trajectories during azeotropic distillation, Chem. Eng. Res. Des. 80 (2002) 654–666.

[13] R. Taylor, H.A. Kooijman, J.S. Hung, A 2nd generation nonequilibrium model for computer-simulation of multicomponent separation processes, Comput. Chem. Eng. 18 (1994) 205–217.

[14] R. Krishnamurthy, R. Taylor, A nonequilibrium stage model of multicomponent separation processes. Part I. Model description and method of solution, AIChEJ 31 (1985) 449–456.

[15] R. Krishnamurthy, R. Taylor, A nonequilibrium stage model of multicomponent separation processes. Part II. Comparison with experiment, AIChEJ 31 (1985) 456–465.

[16] R. Krishnamurthy, R. Taylor, A nonequilibrium stage model of multicomponent separation processes. Part III: the influence of unequal component efficiencies in process design problems, AIChEJ 31 (1985) 1973–1985.

[17] H.D. Mendelson, The prediction of bubble terminal velocities from wave theory, AIChEJ 13 (1967) 250–253.

[18] R. Krishna, M.I. Urseanu, J.M. van Baten, J. Ellenberger, Wall effects on the rise of single gas bubbles in liquids, Int. Commun. Heat Mass Transf. 26 (1999) 781–790.

[19] H.A. Kooijman, R. Taylor, Modeling mass-transfer in multicomponent distillation, Chem. Eng. J. 57 (1995) 177–188.

[20] H.A. Kooijman, R. Taylor, The ChemSep Book, Books on Demand, Norderstedt, Germany, 2001.